Infrared and Raman spectroscopy of $Li_2Ge_7O_{15}$ single crystals: spectra of the paraelectric and aristotype phases

1995 J. Phys.: Condens. Matter 7 5681

(http://iopscience.iop.org/0953-8984/7/28/021)

J. Phys.: Condens. Matter 7 (1995) 5681–5700. Printed in the UK

Infrared and Raman spectroscopy of $Li_2Ge_7O_{15}$ single crystals: spectra of the paraelectric and aristotype phases

V Torgashev†, Yu Yuzyuk†, L Latush†, L Burmistrova†, F Kadlec‡, F Smutný‡ and J Petzelt‡

† Institute of Physics, Rostov State University, Prospekt Stachki 194, 344104 Rostov-on-Don, Russia

‡ Institute of Physics, Academy of Sciences of the Czech Republic, Na Slovance 2, 18040 Praha 8–Libeň, Czech Republic

Received 5 January 1995, in final form 20 March 1995

Abstract. Polarized Raman and infrared spectra of $Li_2Ge_7O_{15}$ single crystals were measured in the frequency range 5–1000 cm^{-1} at room temperature. The spectra are analysed within the framework of the Landau theory of structural phase transitions from a (hypothetical) fully disordered deficient structure (aristotype). The mechanism of the phase transition is discussed in terms of ordering and shifts of ions.

1. Introduction

In the past few years, there has been an increasing amount of experimental evidence and theoretical work that points to peculiar properties of substances called 'weak ferroelectrics', which form a distinct class among ferroelectric crystals. (Let us mention the equivalent concept of 'pseudoproper ferroelectrics' used in the earlier literature.) Weak ferroelectrics are characterized by a low effective charge of the soft mode, which consequently leads to low values of the Curie–Weiss constant and spontaneous polarization. An unusual form of the dielectric susceptibility versus temperature dependence may be encountered here. It was suggested [1] that the smallness of the effective charge of a weakly polar ferroelectric is due to the fact that the mode in question complies to the Brillouin zone centre at an antiferrodistortive transition, which is either a real or a hypothetical precursor of the proper ferroelectric transition.

The aim of this work is investigation of the spectra of one of the representatives of weak ferroelectrics, lithium heptagermanate $Li_2Ge_7O_{15}$ (LGO). The ferroelectric phase transition occurs at $T_c = 283.5$ K [2]. The soft mode was observed by Raman scattering in the ferroelectric phase [3, 4], by infrared (IR) spectroscopy [5, 6] and by hyper Raman scattering [7] in the paraelectric phase; its oscillator strength is extremely small. Critical phenomena are clearly seen [8–10]. Dielectric measurements yielded a low value of the Curie–Weiss constant ($C_{CW} = 4.6$ K); the inverse dielectric susceptibility does not obey the Curie–Weiss law. On cooling, the spontaneous polarization rises to a maximum ($P_{s,max} \simeq 0.03$ μC cm^{-2}, at ~ 260 K), then decreases to zero at $T_z = 135$ K, and below this temperature changes its sign [11–13]. Let us mention that T_z determined in [13] lies considerably lower than that determined in [12].

According to [14], LGO crystals are orthorhombic, with D_{2h}^{14}–$Pbcn$ ($Z = 4$) space group. Though the LGO structure really is orthorhombic, it is a fact that its motif clearly bears the

0953-8984/95/285681+20$19.50

pseudohexagonal character of the GeO_2-type structure. The 'hexagonality' of LGO is also confirmed by numerical values of elastic moduli [2].

The behaviour described above allows one to consider LGO as a member of the class of weak ferroelectrics.

Our work consists of three parts. In the first one, to which this paper is devoted, we show that an aristotype structure of a higher symmetry can be found for LGO and we shall describe the character of the corresponding phase transition. The very existence of this phase transition enables us to describe the origin of the soft mode (which in this case really comes to the Brillouin zone centre of the *Pbcn* phase due to an antiferrodistortive phase transition, thus fulfilling one of the principal requirements of weak ferroelectrics) and to assign the spectrum of the paraelectric phase.

In the second part, entitled 'Disappearance of the IR soft mode in the weak ferroelectric LGO' [24], results of the investigation of the soft mode in the ferroelectric phase are presented and it is shown that the IR oscillator strength of the soft mode turns to zero at about $T_z + \frac{2}{3}(T_c - T_z)$, as assumed by the theory [1]. The last part will deal with hard modes (i.e. the temperature changes of their Raman and IR spectra). Possible mechanisms of the ferroelectric phase transitions will be considered.

2. The crystal structure of LGO and the prototypic phase

Figure 1 shows two projections of the LGO structure constructed using the data from [14, 20]. The crystal is orthorhombic: D_{2h}^{14}–*Pbcn*, with $a = 7.36$, $b = 16.76$ and $c = 9.69$ Å, with four formula units in the elementary cell. The crystal structure is formed by heavily corrugated layers of $[GeO_4]$ tetrahedra bonded together by $[GeO_6]$ octahedra into a three-dimensional network. This structure can be characterized by the formula $Li_2[Ge(Ge_2O_5)_3]$. Li^+ ions are located in channels, as is often encountered within silicate–germanate minerals, but not in ferroelectrics. Let us note that, though the structure is orthorhombic from the crystallographic point of view, substantial features are better perceivable if the structure is derived from a hexagonal quartz-like GeO_2 structure, as indicated in [2]. Analogies between LGO and GeO_2 are as follows:

(i) The lattice constant ratio $b/c \simeq \sqrt{3}$ points to pseudohexagonality.

(ii) GeO_4 tetrahedra are bonded together by a common (shared) oxygen atom into a three-dimensional covalent network.

(iii) Wide channels are formed in the structure along the pseudohexagonal axis.

By contrast, LGO differs from quartz in the following:

(i) There are GeO_6 octahedra in the tetrahedral network of LGO.

(ii) There are Li atoms located in the channels, like in stuffed tridymites.

Li atoms of two sorts (ionized as Li^+) are distributed in channels so that the excess negative charge due to the formation of $[GeO_6]$ octahedra is compensated. Atoms Li1 occupy special 4(b) sites and are coordinated by four oxygen atoms belonging to two $[GeO_6]$ octahedra. Atoms Li2 are placed in a wider channel and are coordinated by two oxygen atoms belonging to one octahedron. This allows one to consider Li2 more loosely bonded in the channel than Li1.

All this shows that the character of LGO structure renders the symmetrization of LGO structure possible. Let us perform such a symmetrization. As seen in figure 1, LGO has two heavily corrugated (hexagonally close-packed) layers formed by oxygen ions (types O2–O5,

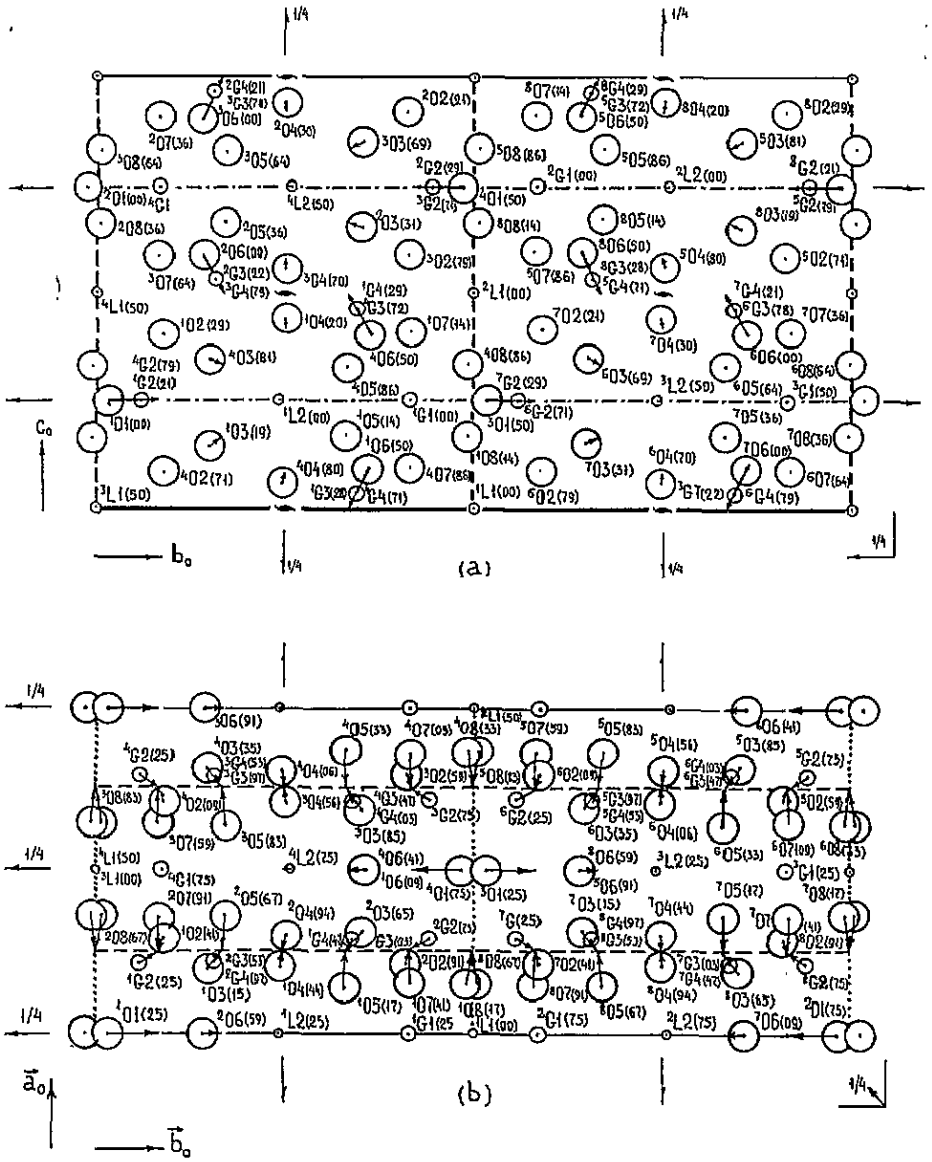

Figure 1. The paraelectric structure of LGO viewed along (*a*) the *a* axis (after [14]) and (*b*) the *c* axis. Arrows indicate symmetrizing shifts; L, G and O stand for lithium, germanium and oxygen, respectively. The third coordinate is given in parentheses (%).

O7 and O8) at elevations close to $a/4$ and $3a/4$. Shifting these ions exactly to positions $a/4$ and $3a/4$ 'flattens' the corrugation. Further let us perform small shifts in the bc plane, as indicated by arrows in figure 1. It is clear that the oxygen atoms in question will then occupy (d) sites of the D_{6h}^4–$P6_3/mmc$ space group, with the unit-cell parameters

$$a^{\mathrm{o}} = c^{\mathrm{h}} \qquad b^{\mathrm{o}} = 6 \times (a^{\mathrm{h}} + b^{\mathrm{h}}) \qquad c^{\mathrm{o}} = 2 \times (b^{\mathrm{h}} - a^{\mathrm{h}}) \tag{1}$$

as shown in figure 2 in thin lines; o and h label the orthorhombic and hexagonal cell, respectively. At this onset, the unit-cell volume ratio $V^{\mathrm{o}}/V^{\mathrm{h}} = 24$. Further symmetrization

of the structure concerns shifts of Li, Ge1, O1 and O6 in the *bc* plane. As the result, these atoms will occupy (a) sites in the hexagonal structure. As depicted in figure 1, the shifts greatest in magnitude concern O1 and O6 and to a lesser extent Li2. Octahedrally coordinated Ge1 and Li1 remain practically unshifted. At these shifts, Ge2–Ge4 (bonded covalently with O1 and O6 to Ge–O–Ge bridges) reach (b) sites of the hexagonal phase. More precisely, to achieve this, small shifts ($\sim$ 0.04 Å) of Ge2–Ge4 atoms along the pseudohexagonal axis are necessary in addition.

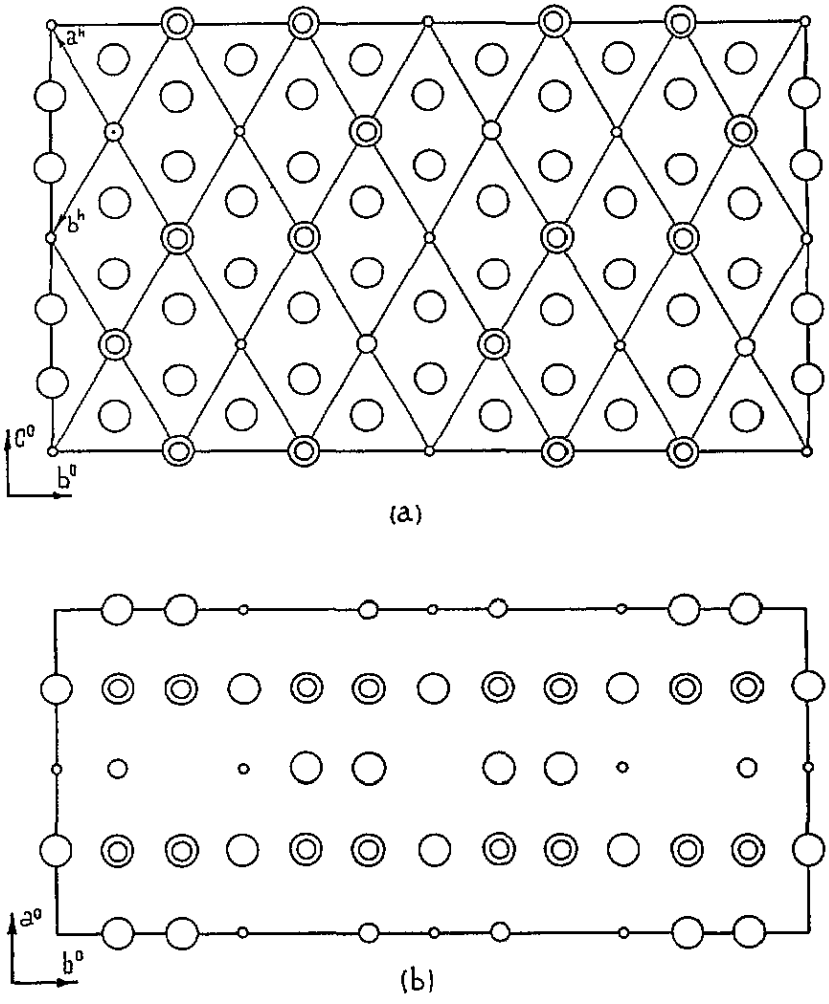

Figure 2. The symmetrized structure of LGO viewed along (*a*) the *a* axis and (*b*) the *c* axis (as in figure 1). Unit cells of $P6_3/mmc$ space group are shown by thin lines.

All the shifts indicated result in the structure drawn in figure 2. Inspection of this figure shows that the prototypic phase of LGO may be presented as a hexagonal close-packed structure of $P6_3/mmc$ symmetry, with disordered octahedral voids. The (a) voids are half-occupied with Li, Ge1, O1 and O6 and half-empty. Ge2–Ge4 atoms occupy (b) sites also with probability 1/2, but the close-packed layers are formed from oxygen atoms O2–O5,

O7 and O8, occupying all the (d) sites. The structural formula of our prototypic phase is thus $(A_{1/2}\square_{1/2})^{(a)}(B_{1/2}\square_{1/2})^{(b)}O_2^{(d)}$; $\square$ stands for void; A for Li, Ge1, O1, O6; and B for Ge2–Ge4. Table 1 gives generalized data on the occupancy of sites in the prototypic and the orthorhombic phases, and their transformations.

3. Group-theoretical analysis and mechanism of the $D_{6h}^4 \rightarrow D_{2h}^{14}$ phase transition

To describe the hypothetical phase transition introduced we shall employ the usual Landau group-theoretical approach [15]. (Let us mention that the monograph [15] outlines exhaustively the treatment of phase transitions from the close-packed A1 and A3 structures—with symmetry O_h^5 and D_{6h}^4, respectively—based on extended ideas of Landau theory; phases of a substance with symmetries connected by group–subgroup relations are called 'Landau phases'.) As shown above, the relation of D_{6h}^4 and D_{2h}^{14} lattice parameters is determined by relations (1). Such a 24-fold multiplication of the unit-cell volume allows us to select unambiguously the star of vectors $\{k\}$ of the prototypic phase, according to which the phase transition can be realized. Figure 3 shows how the orthorhombic reciprocal cells are embedded in the hexagonal one. Obviously, the star $\{k\}$ of vectors that play a role in the phase transition is reducible and consists of two irreducible stars (throughout this paper we label wavevectors and irreducible representations according to Kovalev [16]): $\{k_5 = \frac{1}{4}b_1\}$ and $\{k_6 = \frac{1}{12}(b_1 + b_2)\}$. It is seen in figure 3 that four arms only (two arms per star) out of all the arms of these two six-arm stars participate in the phase transition: k_6^1, k_6^4, k_5^3 and k_5^6. According to [16], four irreducible representations correspond to each of these stars: Σ_1–Σ_4 to $\{k_5\}$ and T_1–T_4 to $\{k_6\}$. The labelling of reciprocal space points we use complies with the one adopted generally [17]. To find the order parameter appropriate for the phase transition considered, it is necessary to inspect 16 combinations of reducible representations $\Sigma_i \oplus T_j$ ($i, j = 1$–4). We performed this cumbersome work; the final result is presented in table 2, which lists possible space groups of the low-symmetry phases (having Γ° lattice and belonging to the D_{2h} class) that are of interest. Leftwards and upwards from irreducible representations the space groups are given (if the order parameter transforms according to the corresponding irreducible representations). Resulting multiplications of the unit-cell volume are, however, smaller than the real one (24-fold) we have in LGO; this fact speaks for the necessity of introducing a reducible star. Rightwards and downwards from the representations, there are 32 phases with 24-fold volume multiplication. The group D_{2h}^{14} appears here four times: two cases from $\Sigma_3 \oplus T_2$ and the two others from $\Sigma_2 \oplus T_4$. But in the case of $\Sigma_2 \oplus T_4$ the n plane is perpendicular to the hexade, which is not in accord with the situation in LGO. We may thus conclude that we determined unambiguously the order parameter of the $D_{6h}^4 \rightarrow D_{2h}^{14}$ phase transition in LGO. This order parameter transforms according to $\Sigma_3 \oplus T_2$.

The group-theoretical analysis performed shows that this order parameter allows 56 phases (considering all the arm combinations). Out of these, the phases with *Pbcn* symmetry appear in two solutions of state equations. (Because of that table 2 shows two identical space groups.) Subsequent detailed analysis of the ordering we actually see in LGO, however, excludes one solution as unmatching. Thus, only one solution of the state equations ($\Delta\rho$) suits the case of LGO: $k_5 = (0, 0, \eta, 0, 0, -\eta)$ and $k_6 = (\xi, 0, 0, e^{i2\pi/3}\xi, 0, 0)$.

The generators of $\Sigma_3 \oplus T_2$ representation of the group D_{6h}^4 are:

Table 1. Transformation of Wyckoff positions and mechanical representation at $P6_3/mmc \rightarrow Pbcn$ phase transition for LGO. Order parameter is $\tau_3[k_5 = \frac{1}{4}b_1]\oplus\tau_2[k_6 = \frac{1}{12}(b_1+b_2)]$. Assignments: h($i$) marks void in ($i$) Wyckoff position; so = site occupancy; NDF (E)UC = the number of degrees of freedom for (extended) unit cell.

$P6_3/mmc$–D^4_{6h}					$P2_1/b2/c2_1/n$–D^{14}_{2h}				
Wyckoff position	Ion	so	NDF EUC	Mechanical representation for points that transformed to Γ point *Pbcn* phase at D^4_{6h}–D^{14}_{2h} phase transition	Wyckoff position	Ion	so	NDF UC	Mechanical representation for Γ point
D_{3d} (2):(a)	O	1/4	36	$1(\Gamma_4+\Gamma_8+\Gamma_{10}+\Gamma_{12})+$	C_i(4):(a)	h(a)	1	12	$3A_u+3B_{1u}+3B_{2u}+3B_{3u}$
	Li	1/6	24	$2(2\Sigma_1+\Sigma_2+\Sigma_3+2\Sigma_4)+$	C_i(4):(b)	Li1	1	12	$3A_u+3B_{1u}+3B_{2u}+3B_{3u}$
	Ge	1/12	12	$3(M_2+2M_4+M_6+2M_8)+$	C_2^y(4):(c)	Li2	1	12	$A_g+A_u+2B_{1g}+2B_{1u}+B_{2g}+B_{2u}+2B_{3g}+2B_{3u}$
	h(a)	1/2	72	$10(T_1+T_2+2T_3+2T_4)+$	C_2^y(4):(c)	Ge1	1	12	$A_g+A_u+2B_{1g}+2B_{1u}+B_{2g}+B_{2u}+2B_{3g}+2B_{3u}$
				$2(K_3+K_4+K_5+K_6)+$	C_2^y(4):(c)	O1	1	12	$A_g+A_u+2B_{1g}+2B_{1u}+B_{2g}+B_{2u}+2B_{3g}+2B_{3u}$
				$2(T'_1+T'_2+2T'_3+2T'_4)+$	C_2^y(4)(c)	h(c)1	1	12	$A_g+A_u+2B_{1g}+2B_{1u}+B_{2g}+B_{2u}+2B_{3g}+2B_{3u}$
				$4(2\tau_1+4\tau_2)$	C_2^y(4):(c)	h(c)2	1	12	$A_g+A_u+2B_{1g}+2B_{1u}+B_{2g}+B_{2u}+2B_{3g}+2B_{3u}$
					C_2^y(4):(c)	h(d)3	1	12	$A_g+A_u+2B_{1g}+2B_{1u}+B_{2g}+B_{2u}+2B_{3g}+2B_{3u}$
					C_1(8):(d)	O6	1	24	$3A_g+3A_u+3B_{1g}+3B_{1u}+3B_{2g}+3B_{2u}+3B_{3g}+3B_{3u}$
					C_1(8):(d)	h(d)0	1	24	$3A_g+3A_u+3B_{1g}+3B_{1u}+3B_{2g}+3B_{2u}+3B_{3g}+3B_{3u}$
D'_{3h}(2):(b)	Ge	1/2	72	$1(\Gamma_4+\Gamma_5+\Gamma_{10}+\Gamma_{11})+$	C_1(8):(d)	Ge2	1	24	$3A_g+3A_u+3B_{1g}+3B_{1u}+3B_{2g}+3B_{2u}+3B_{3g}+3B_{3u}$
	h(b)	1/2	72	$2(2\Sigma_1+2\Sigma_3+2\Sigma_4)+$	C_1(8):(d)	Ge3	1	24	$3A_g+3A_u+3B_{1g}+3B_{1u}+3B_{2g}+3B_{2u}+3B_{3g}+3B_{3u}$
				$3(M_1+M_3+M_4+M_5+M_6+M_8)+$	C_1(8):(d)	Ge4	1	24	$3A_g+3A_u+3B_{1g}+3B_{1u}+3B_{2g}+3B_{2u}+3B_{3g}+3B_{3u}$
				$10(2T_1+T_2+2T_3+T_4)+$	C_1(8):(d)	h(d)1	1	24	$3A_g+3A_u+3B_{1g}+3B_{1u}+3B_{2g}+3B_{2u}+3B_{3g}+3B_{3u}$
				$2(K_1+K_3+K_5+K_6)+$	C_1(8):(d)	h(d)2	1	24	$3A_g+3A_u+3B_{1g}+3B_{1u}+3B_{2g}+3B_{2u}+3B_{3g}+3B_{3u}$
				$2(2T'_1+T'_2+2T'_3+T'_4)+$	C_1(8):(d)	h(d)3	1	24	$3A_g+3A_u+3B_{1g}+3B_{1u}+3B_{2g}+3B_{2u}+3B_{3g}+3B_{3u}$
				$4(4\tau_1+2\tau_2)$					
D'_{3h}(2):(d)	O	1	144	$1(\Gamma_4+\Gamma_5+\Gamma_{10}+\Gamma_{11})+$	C_1(8):(d)	O2	1	24	$3A_g+3A_u+3B_{1g}+3B_{1u}+3B_{2g}+3B_{2u}+3B_{3g}+3B_{3u}$
				$2(2\Sigma_1+2\Sigma_3+2\Sigma_4)+$	C_1(8):(d)	O3	1	24	$3A_g+3A_u+3B_{1g}+3B_{1u}+3B_{2g}+3B_{2u}+3B_{3g}+3B_{3u}$
				$3(M_1+M_3+M_4+M_5+M_6+M_8)+$	C_1(8):(d)	O4	1	24	$3A_g+3A_u+3B_{1g}+3B_{1u}+3B_{2g}+3B_{2u}+3B_{3g}+3B_{3u}$
				$10(2T_1+T_2+2T_3+T_4)+$	C_1(8):(d)	O5	1	24	$3A_g+3A_u+3B_{1g}+3B_{1u}+3B_{2g}+3B_{2u}+3B_{3g}+3B_{3u}$
				$2(K_1+K_3+K_5+K_6)+$	C_1(8):(d)	O7	1	24	$3A_g+3A_u+3B_{1g}+3B_{1u}+3B_{2g}+3B_{2u}+3B_{3g}+3B_{3u}$
				$2(2T'_1+T'_2+2T'_3+T'_4)+$	C_1(8):(d)	O8	1	24	$3A_g+3A_u+3B_{1g}+3B_{1u}+3B_{2g}+3B_{2u}+3B_{3g}+3B_{3u}$
				$4(4\tau_1+2\tau_2)$					

Table 2. Space groups of D_{2h} low-symmetry phases with Γ_0 lattice for order parameter, which is transformed by the $\tau_i(k_5) + \tau_j(k_6)$ reducible representations of $P6_3/mmc$ space group.

	$k_6 = \frac{1}{12}(b_1 + b_2)$	$P\frac{2}{b}\frac{2_1}{c}\frac{2_1}{m}$–$D_{2h}^{11}$ $P\frac{2_1}{m}\frac{2}{m}\frac{2}{a}$–$D_{2h}^{5}$	$P\frac{2_1}{b}\frac{2}{c}\frac{2_1}{n}$–$D_{2h}^{14}$ $P\frac{2}{m}\frac{2}{n}\frac{2_1}{a}$–$D_{2h}^{7}$	$P\frac{2_1}{n}\frac{2_1}{m}\frac{2_1}{a}$–$D_{2h}^{16}$ $P\frac{2_1}{m}\frac{2_1}{m}\frac{2}{n}$–$D_{2h}^{13}$	$P\frac{2}{b}\frac{2_1}{c}\frac{2_1}{m}$–$D_{2h}^{11}$ $P\frac{2_1}{b}\frac{2_1}{c}\frac{2_1}{a}$–$D_{2h}^{15}$
$k_5 = \frac{1}{4}(b_1)$		T_1	T_2	T_3	T_4
$P\frac{2_1}{m}\frac{2}{m}\frac{2}{a}$–$D_{2h}^{5}$	Σ_1	$P\frac{2_1}{m}\frac{2}{m}\frac{2}{a}$–$D_{2h}^{5}$	$P\frac{2}{m}\frac{2}{n}\frac{2_1}{a}$–$D_{2h}^{7}$	$P\frac{2_1}{m}\frac{2_1}{m}\frac{2}{n}$–$D_{2h}^{13}$	$P\frac{2}{b}\frac{2_1}{c}\frac{2_1}{m}$–$D_{2h}^{11}$
$P\frac{2_1}{m}\frac{2_1}{m}\frac{2}{n}$–$D_{2h}^{13}$		$P\frac{2_1}{m}\frac{2}{m}\frac{2}{a}$–$D_{2h}^{5}$	$P\frac{2}{m}\frac{2}{n}\frac{2_1}{a}$–$D_{2h}^{7}$	$P\frac{2_1}{m}\frac{2_1}{m}\frac{2}{n}$–$D_{2h}^{13}$	$P\frac{2}{b}\frac{2_1}{c}\frac{2_1}{m}$–$D_{2h}^{11}$
$P\frac{2_1}{c}\frac{2}{c}\frac{2}{a}$–$D_{2h}^{8}$	Σ_2	$P\frac{2_1}{c}\frac{2}{c}\frac{2}{a}$–$D_{2h}^{8}$	$P\frac{2}{n}\frac{2_1}{n}\frac{2}{a}$–$D_{2h}^{6}$	$P\frac{2_1}{c}\frac{2_1}{c}\frac{2}{n}$–$D_{2h}^{10}$	$P\frac{2_1}{b}\frac{2}{c}\frac{2_1}{n}$–$D_{2h}^{14}$
$P\frac{2_1}{c}\frac{2_1}{c}\frac{2}{n}$–$D_{2h}^{10}$		$P\frac{2_1}{c}\frac{2}{c}\frac{2}{a}$–$D_{2h}^{8}$	$P\frac{2}{n}\frac{2_1}{n}\frac{2}{a}$–$D_{2h}^{6}$	$P\frac{2_1}{c}\frac{2_1}{c}\frac{2}{n}$–$D_{2h}^{10}$	$P\frac{2_1}{b}\frac{2}{c}\frac{2_1}{n}$–$D_{2h}^{14}$
$P\frac{2}{b}\frac{2_1}{c}\frac{2_1}{m}$–$D_{2h}^{11}$	Σ_3	$P\frac{2}{b}\frac{2_1}{c}\frac{2_1}{m}$–$D_{2h}^{11}$	$P\frac{2_1}{b}\frac{2}{c}\frac{2_1}{n}$–$D_{2h}^{14}$	$P\frac{2_1}{n}\frac{2_1}{m}\frac{2_1}{a}$–$D_{2h}^{16}$	$P\frac{2_1}{b}\frac{2_1}{c}\frac{2_1}{a}$–$D_{2h}^{15}$
$P\frac{2_1}{n}\frac{2_1}{m}\frac{2_1}{a}$–$D_{2h}^{16}$		$P\frac{2}{b}\frac{2_1}{c}\frac{2_1}{m}$–$D_{2h}^{11}$	$P\frac{2_1}{b}\frac{2}{c}\frac{2_1}{n}$–$D_{2h}^{14}$	$P\frac{2_1}{n}\frac{2_1}{m}\frac{2_1}{a}$–$D_{2h}^{16}$	$P\frac{2_1}{b}\frac{2_1}{c}\frac{2_1}{a}$–$D_{2h}^{15}$
$P\frac{2_1}{b}\frac{2_1}{a}\frac{2}{m}$–$D_{2h}^{9}$	Σ_4	$P\frac{2_1}{b}\frac{2_1}{a}\frac{2}{m}$–$D_{2h}^{9}$	$P\frac{2_1}{n}\frac{2_1}{n}\frac{2}{m}$–$D_{2h}^{12}$	$P\frac{2_1}{n}\frac{2_1}{m}\frac{2_1}{a}$–$D_{2h}^{16}$	$P\frac{2_1}{n}\frac{2_1}{m}\frac{2_1}{a}$–$D_{2h}^{16}$
$P\frac{2_1}{n}\frac{2_1}{m}\frac{2_1}{a}$–$D_{2h}^{16}$		$P\frac{2_1}{b}\frac{2_1}{a}\frac{2}{m}$–$D_{2h}^{9}$	$P\frac{2_1}{n}\frac{2_1}{n}\frac{2}{m}$–$D_{2h}^{12}$	$P\frac{2_1}{n}\frac{2_1}{m}\frac{2_1}{a}$–$D_{2h}^{16}$	$P\frac{2_1}{n}\frac{2_1}{m}\frac{2_1}{a}$–$D_{2h}^{16}$

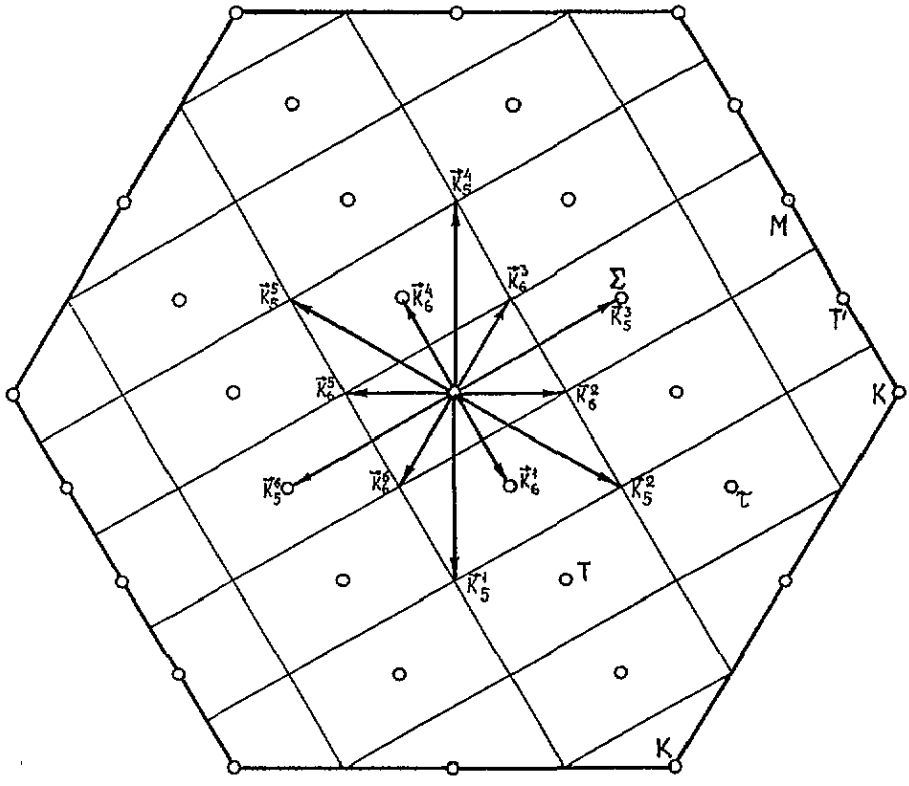

Figure 3. Relations between Brillouin zones of $P6_3/mmc$ and $Pbcn$ phases of LGO. Arrows: rays of $\{k_5\}$ and $\{k_6\}$ stars; circles: points of the hexagonal zone that transform to the centre of zone of the D_{2h}^{14} phase at the $D_{6h}^{4} \rightarrow D_{2h}^{14}$ phase transition.

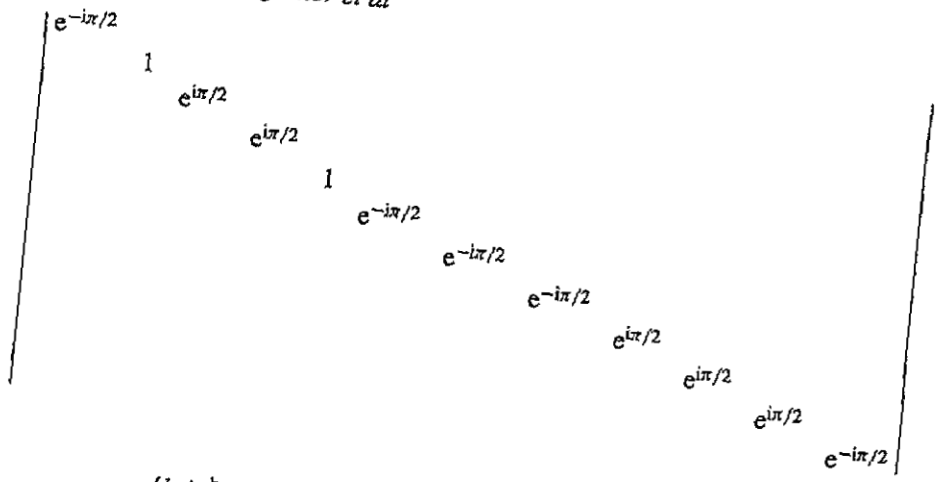

$\{h_1|a^h\}$

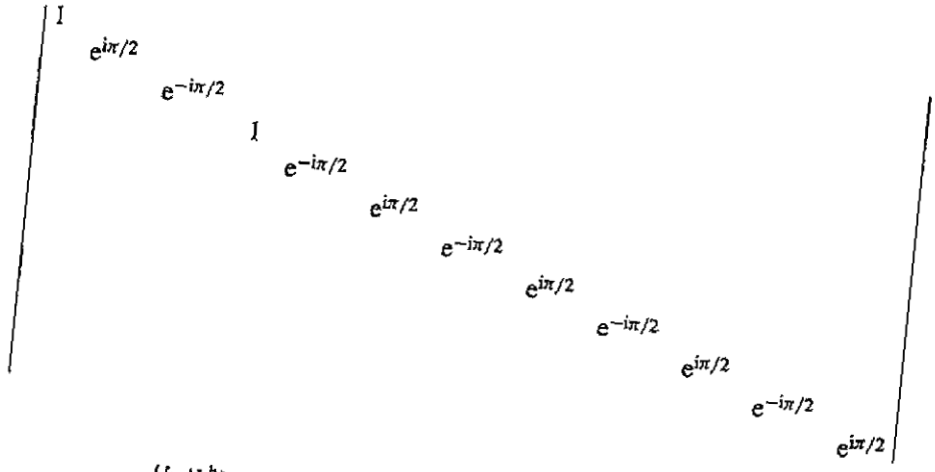

$\{h_1|b^h\}$

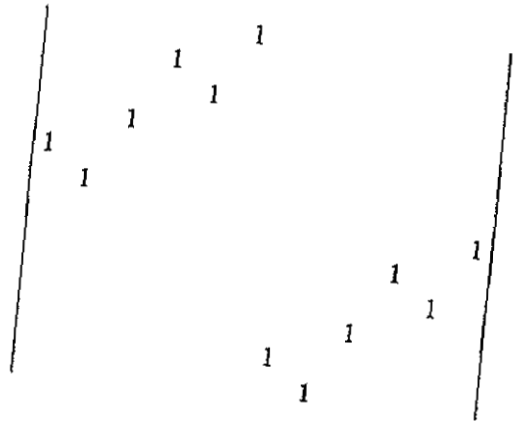

$\{h_2|c^h/2(\equiv \tau_z)\}$

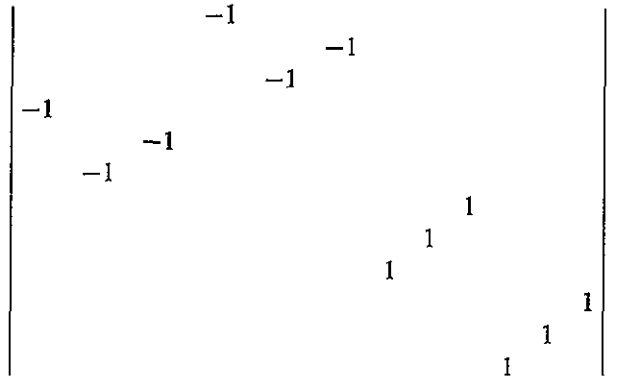

$\{h_7|0\}$

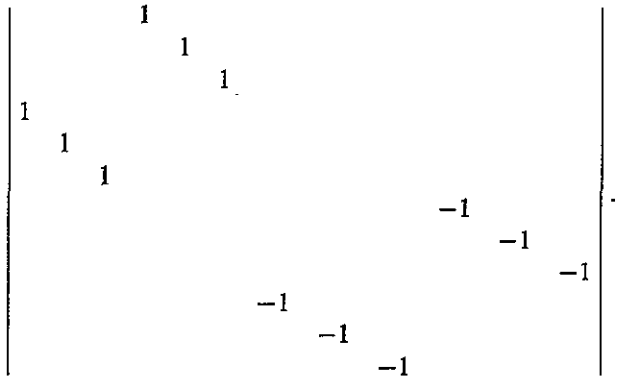

$\{h_{13}|0\}$

Correspondence between symmetry elements of D_{6h}^4 and D_{2h}^{14} reads:

$\{h_1|000\} \rightarrow E$

$\{h_4|a^h - 5b^h + c^h/2\} \rightarrow C_2^x(2_1)$

$\{h_{11}|000\} \rightarrow C_2^y(2)$

$\{h_8|a^h - 5b^h + c^h/2\} \rightarrow C_2^z(2_1)$

$\{h_{13}|2a^h\} \rightarrow I$ (inversion)

$\{h_{16}|a^h - 5b^h + c^h/2\} \rightarrow \sigma^{yz}$ (b plane)

$\{h_{23}|2b^h\} \rightarrow \sigma^{xz}$ (c plane)

$\{h_{20}|a^h - 5b^h + c^h/2\} \rightarrow \sigma^{xy}$ (n plane).

Just for this solution, the ordering shown in figure 2 was obtained.

Let us show that the symmetrization of LGO structure we performed entirely 'by hand' corresponds to the backward process that takes place at the phase transition. In other words, we shall show that the symmetry of order parameter introduced allows us to describe the transformation of the aristotype structure to the real LGO. This task we fulfilled by checking the 'activity' of $\Sigma_3 \oplus T_2$ representation with respect to ordering and displacement mechanisms (what we did 'by hand'). Such a check is done with the help of orthogonality

relations for characters [15]. It allows us to determine whether the representation in question is contained in the representation of the suggested model of charge-density distribution probability change and, if yes, how many times.

The representation of the transition model we investigate is a product of three representations: a representation of the subgroup of translations, a permutational representation and displacive representations (T_z and T_{xy}). Having constructed these representations and having decomposed them into irreducible ones, we arrived at results presented in table 3. From there it follows that the corresponding ordering in LGO according to (a) sites is given by T_2 representation, which encompasses xy shifts of (a) sites and z shifts of (d) and (b) sites. Representation Σ_3 is responsible only for shifts of (a), (b) and (d) sites in the plane perpendicular to hexade. Table 3 also shows that neither Σ_3 nor T_2 is active in ordering of (b) sites (figure 2 indicates that the (b) sites also order). To remedy this, it is necessary to inspect which representation out of those active in (b) ordering (Σ_1, T_1, T_3) does not violate the order parameter symmetry (i.e. which one is a secondary non-symmetry-breaking order parameter). A correlation of irreducible representations from all points of the D_{6h}^4 phase that fold into the Brillouin zone centre due to the phase transition is presented in figure 4. From there it follows that the secondary order parameter belongs to the representation T_1 ($k_6 = \frac{1}{6}(b_1 + b_2)$), which really is active in ordering of (b) sites. This secondary order parameter takes care of ordering of Ge2–Ge4 atoms, which actually occurs in the *Pbcn* phase of LGO.

Table 3. Decomposition of the arrangement (OD) and the shift (T_z, T_{xy}) representations at (a), (b) and (d) Wyckoff positions of D_{6h}^4 space group into irreducible representations.

IR	(a)			(b)			(d)		
	OD	T_z	T_{xy}	OD	T_z	T_{xy}	OD	T_z	T_{xy}
Σ_1	1	1	1	2	—	2	2	—	2
Σ_2	—	—	1	—	—	—	—	—	—
Σ_3	—	—	1	—	—	2	—	—	2
Σ_4	1	1	1	—	2	—	—	2	—
T_1	1	—	1	1	—	2	1	—	2
T_2	1	—	1	—	1	—	—	1	—
T_3	—	1	1	1	—	2	1	—	2
T_4	—	1	1	—	1	—	—	1	—

4. Phonon spectrum of *Pbcn* phase of LGO

Figures 5 and 6 present polarized Raman and IR reflectivity spectra of an LGO single crystal taken at 290 K and 300 K, respectively, which may serve us in working out symmetry relations for modes of the D_{2h} factor group. (Unfortunately, the only LGO ($E \| a$) sample we had at our disposal for IR reflectivity measurements was too small to yield a good low-noise spectrum. Because of that figure 6 is not complete.) The mode frequencies are presented in table 4. The spectrum is clearly divided into two regions: 0–600 and 780–950 cm^{-1}. Apparently, the higher-frequency modes correspond to stretch vibrations of covalent Ge–O bonds. Deformation modes and lattice modes have practically no gap and, most likely, a 'molecular' approximation is of no value here. We thus think that a routine assignment of

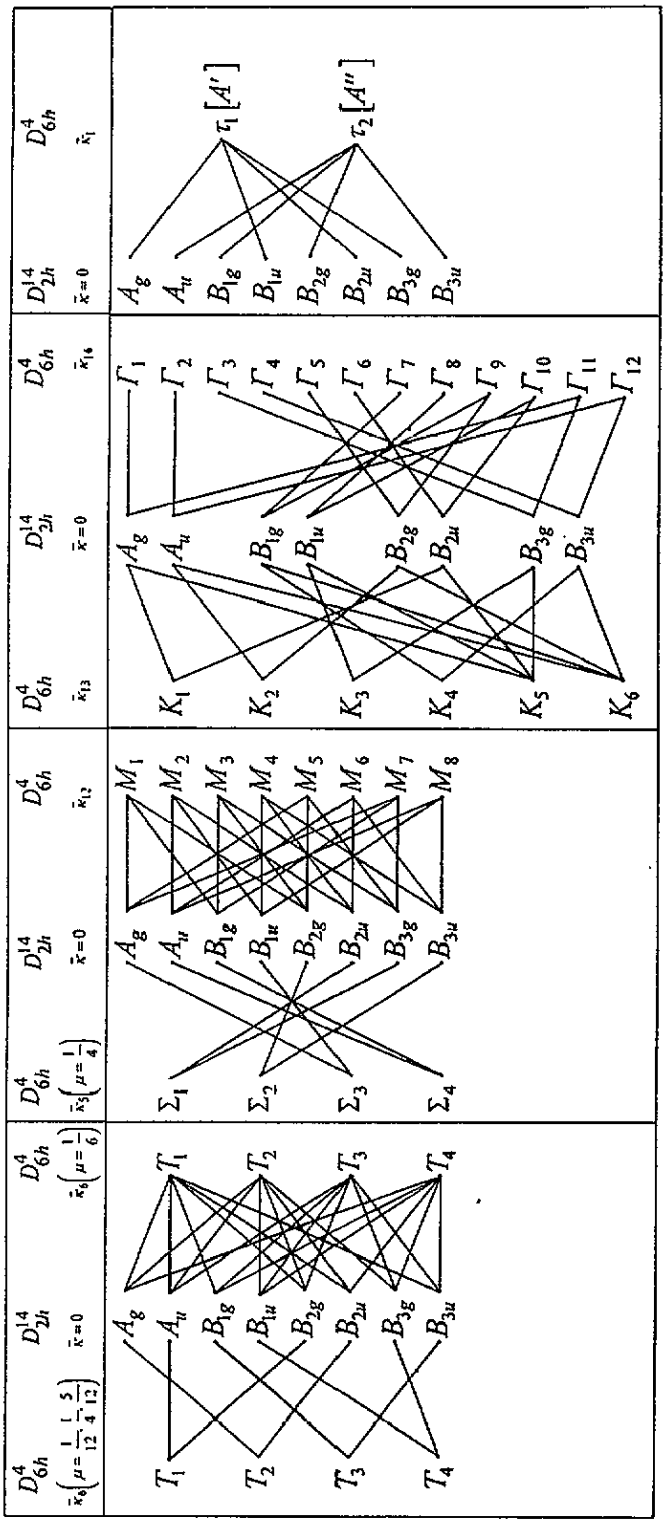

Figure 4. Compatibility relations between irreducible representations of D^4_{6h} and D^{14}_{2h} space groups for LGO.

Table 4. Frequencies of lines in the Raman and IR spectra of LGO single crystals at room temperature: exp(erimental); est(imated). Assignments are labelled according to figure 7.

A_g(aa, bb, cc)		B_{1g}(ab)		B_{2g}(ac)		B_{3g}(bc)		A_u(–)		B_{1u}(c)		B_{2u}(b)		B_{3u}(a)		Assignments and comments
exp	est	exp	est	exp	est	exp	est	exp	est	exp	est	exp	est	exp	est	
—	—	—	—	—	—	—	—	—	—	—	0	—	0	—	0	$\Gamma_4(x)$; $\Gamma_{10}(yz)$
53	50	—	—	—	—	—	—	—	—	7	50	—	—	—	—	$\Sigma_3(1/4)$; TA(yz);SM
—	—	—	—	—	—	—	55	—	—	50	55	—	—	—	—	$T_4(1/12)$; TA(x)
—	—	45	60	52	60	53	60	—	—	—	—	—	—	—	—	M_3; TA(yz)
—	—	51	61	—	—	—	—	—	—	—	—	—	—	—	61	$T_3(1/12)$; TA(yz)
—	—	—	—	61	69	—	—	—	69	—	—	—	—	—	—	$T_1(1/12)$; TA(yz)
68	70	—	—	—	—	68	70	—	—	—	—	—	—	—	—	Γ_{11}; TO(yz); RLM
—	—	68	75	—	—	—	—	—	—	—	—	—	—	—	75	$T_3(1/12)$; TO(yz)
—	85	—	—	—	—	76	85	—	—	—	85	—	85	—	—	$\tau_1(1)$; TA(yz)
—	—	86	90	—	—	—	—	—	90	—	—	—	—	—	—	$\Sigma_4(1/4)$; TA(x)
—	—	—	—	—	—	—	98	—	—	—	—	—	98	—	—	$\Sigma_1(1/4)$; LA(yz)
—	—	—	99	90	99	—	99	—	99	—	99	—	—	—	99	$T_3(1/6)$; TA(yz)
—	—	—	100	—	—	—	—	—	—	—	—	—	—	—	100	$T_3(5/12)$
—	100	—	—	—	—	—	100	—	—	—	100	—	100	—	—	$\tau_1(2)$; TA(yz)
—	102	101	102	—	—	103	102	—	—	—	102	—	102	—	102	$T_4(1/6)$; TA(x)
109	106	108	106	109	106	—	—	—	—	—	—	—	—	—	—	M_1; LA(yz)
111	107	—	—	—	—	—	—	—	—	—	107	—	—	—	—	$\Sigma_3(1/4)$; TO(yz)
112	110	—	110	—	110	—	—	—	110	—	—	—	110	—	110	$T_1(1/6)$; LA(yz)
—	—	—	—	—	112	—	—	—	112	—	—	—	—	—	—	$T_1(1/12)$; LO(yz)
—	—	—	—	—	114	—	—	—	114	—	—	—	—	—	—	$T_1'(5/12)$
—	—	—	115	—	—	—	—	—	—	—	—	—	—	—	115	$T_3(1/4)$; TA(yz)
—	—	—	116	117	116	—	116	—	116	—	116	—	—	—	116	$T_3(1/6)$; TO(yz)
—	—	—	—	—	120	—	—	—	120	—	—	—	—	—	—	$T_1(1/4)$; LA(yz)
—	—	131	125	—	125	—	—	—	125	—	—	—	—	—	125	$\tau_2(1)$; TA(x)
131	130	—	—	—	—	133	130	—	—	—	130	—	130	—	—	K_5; (LA+TA)(yz)
—	—	—	—	—	—	—	—	—	—	—	131	—	131	146	131	M_4; TA(x)
—	—	—	—	—	—	—	132	—	—	—	132	—	—	—	—	$T_4(1/4)$; TA(x)
—	—	—	—	—	—	—	138	—	—	—	138	—	—	—	—	$T_4'(5/12)$
—	—	—	142	—	142	—	—	—	142	—	—	—	—	155	142	K_6; TA(x)+LO(x)

Table 4. (Continued)

A_g(aa, bb, cc)		B_{1g}(ab)		B_{2g}(ac)		B_{3g}(bc)		A_u(–)		B_{1u}(c)		B_{2u}(b)		B_{3u}(a)		Assignments and comments
exp	est	exp	est	exp	est	exp	est	exp	est	exp	est	exp	est	exp	est	
—	—	—	—	—	—	—	—	—	144	—	—	—	144	167	144	M_6; TO(yz)
—	145	—	—	—	—	—	145	—	—	—	145	—	145	—	—	$\tau_1(1)$; TO(yz)
—	—	—	150	—	150	—	—	—	150	—	—	—	—	—	150	$\tau_2(2)$; TO(x)
156	150	—	—	—	—	—	—	—	—	—	—	—	150	—	—	$T_2(1/4)$; LO(x)
—	—	—	—	—	152	—	—	—	152	—	—	—	—	—	—	$T_1'(5/12)$
—	—	157	155	—	—	—	—	—	—	—	—	—	—	—	155	$T_3(1/4)$; TO(yz)
—	—	—	—	—	—	172	160	—	—	158	160	—	—	—	—	K_3; TO(yz)
—	161	—	—	—	—	—	—	—	—	—	—	—	161	—	—	$T_2'(5/12)$
164	163	—	—	—	163	186	163	—	163	195	163	163	163	—	—	$T_2(1/6)$; LO(x)
—	—	172	171	—	—	—	—	—	171	—	—	—	—	—	—	$\Sigma_4(1/4)$; LO(x)
186	180	—	—	—	—	—	—	—	—	—	—	—	180	—	—	$T_2(1/12)$; LO(x)
192	181	—	—	181	181	201	181	—	—	—	—	—	—	—	—	M_5; LO(x)
—	—	—	—	—	—	212	193	—	—	—	—	190	193	—	—	$\Sigma_1(1/4)$; LO(yz)
—	—	—	—	208	196	—	—	—	—	—	—	—	—	—	—	Γ_5; LO(x); RLM
203	205	189	205	—	205	—	—	—	205	—	—	216	205	196	205	$T_1(1/6)$; LO(yz)
—	—	200	—	—	—	—	—	—	—	—	—	—	—	—	—	?
214	—	215	—	—	—	—	—	—	—	—	—	—	—	—	—	?
223	—	223	—	225	—	—	—	—	—	226	—	—	—	220	—	?
228	—	237	—	—	—	—	—	—	—	—	—	—	—	—	—	?
—	—	—	—	—	—	—	—	—	260	239	260	—	—	252	260	M_8; LO(yz)
—	—	255	—	253	—	252	—	—	—	—	—	—	—	—	—	?
260	260	—	—	—	—	263	260	—	—	273	260	262	260	—	—	$\tau_1(2)$; TO(yz)
—	—	260	—	—	—	—	—	—	—	—	—	—	—	—	—	?
—	—	274	270	—	—	—	—	—	—	—	—	—	—	271	270	$T_3'(5/12)$
272	—	—	—	272	—	—	—	—	—	—	—	279	—	—	—	?
—	—	—	—	287	280	—	—	—	280	—	—	—	—	—	—	$T_1(1/4)$; LO(yz)
289	295	—	—	—	—	—	—	—	—	—	—	297	295	—	—	K_1; LO(yz)
—	—	291	—	—	—	287	—	—	—	289	—	—	—	—	—	?
17	18	18	18	11	18	12	18	0	18	8	18	6	18	7	18	All together

lines for LGO, based on molecular approximation carried out without theoretical calculations (e.g. by the method of translationally symmetric vibrational coordinates taking into account mechanical interactions between vibrations of complex anions and lattice vibrations [18]) would turn out to be quite speculative (and giving not much information). Owing to the complexity of LGO structure, i.e. the existence of a tremendously high number of degrees of freedom, even such theoretical calculations may nevertheless lead to ambiguous conclusions.

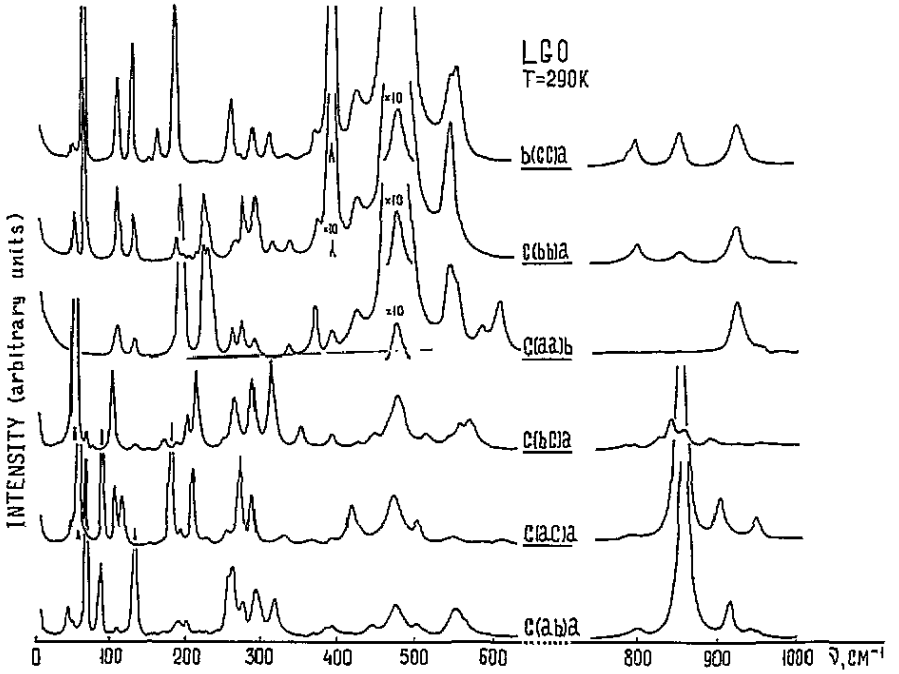

Figure 5. Raman spectra of LGO single crystal at 290 K.

The hypothetical structure we derived, however, possesses a unit cell of much smaller volume, which fact allows one to shorten considerably the burden of numerical work in calculating phonon dispersion curves. Knowing the $D_{6h}^4 \rightarrow D_{2h}^{14}$ phase transition mechanism, we can determine the dispersion curves of the D_{2h}^{14} phase by their folding transformation from curves of the D_{6h}^4 phase. Figure 3 shows that the following points of the D_{6h}^4 phase fold to the centre of the Brillouin zone for D_{2h}^{14}: one Γ point, two Σ points, three M points, ten T points, two T' points, two K points and (lastly) four τ points of general direction in reciprocal space (24 points in total). These points are marked with circles in figure 3. By determining the composition of mechanical representation for these points and correlating irreducible representations of D_{6h}^4 and D_{2h}^{14} one can grasp the genesis of vibrational spectra of real LGO from its hypothetical structure. We undertook this procedure; the results are shown in table 1. Numbers standing in front of parentheses with D_{6h}^4 phase representations correspond to the number of points folding to the centre of *Pbcn* Brillouin zone at the transition. Let us note that the total mechanical representation is in a way 'overcrowded': it incorporates vibrational degrees of freedom of voids in (a) and (b) sites. Since only one-half of (a) and (b) sites is populated with real ions, only one-half of degrees of freedom for (a) and (b) sites of the enlarged cell corresponds to vibrations of real particles. It follows from

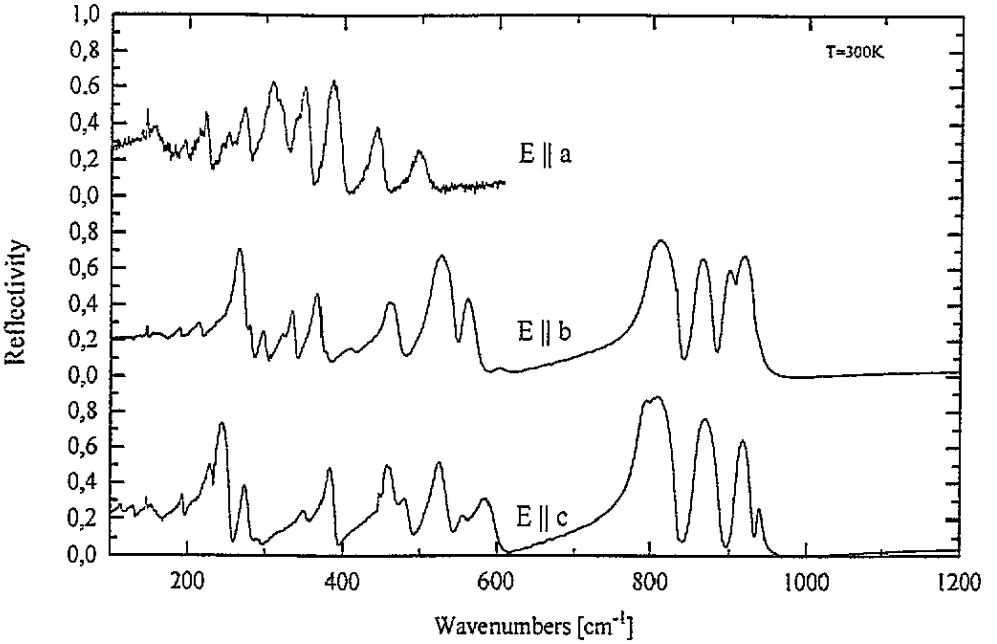

Figure 6. IR reflectivity spectra of LGO single crystal at 300 K.

the right-hand part of table 1 that, for both (a) and (b) sites, the degrees of freedom at the $D_{6h}^4 \rightarrow D_{2h}^{14}$ transition are distributed strictly symmetrically between vacancies and ions (share and share alike), so that the sets of mechanical representations of vacancies and real ions are identical.

Since the (d) site of D_{6h}^4 phase is fully populated, it can be considered in essence that vibrations of (d) oxygens in the two close-packed layers form a regular low-frequency phonon spectrum of such a crystal. Within this spectrum, doubly degenerate transverse shear modes (vibrations perpendicular to the hexade) and non-degenerate compressional modes (vibrations along the hexade) may be selected. Microscopical calculations are necessary to determine the character of phonon dispersions $\omega(q)$; their qualitative picture can nevertheless be arrived at by taking into consideration the known room-temperature values of elastic moduli [2] and experimental vibrational spectra (an analogous procedure is described in [19] in more detail). Figure 7 shows possible ordering of low-frequency dispersion curves for the prototypic phase of LGO. Correlations between irreducible representations of D_{6h}^4 are given in figure 8. The relatively low value of the shear mode Γ_{11} requires formation of layers in LGO structure, perpendicularly to the hexagonal axis. It also follows from figure 7 that the spectrum of *Pbcn* phase below 300 cm^{-1} is formed principally of oxygen layer vibrations (with bonds of an ionic character).

At our phase transition, a zone folding occurs and points of dispersion curves (marked with dots) fold into the centre of the low-symmetry Brillouin zone (see figure 9). There, the highest degeneracy of the vibrational term (sixfold) occurs for the T modes and $q = \frac{1}{6}(b_1 + b_2)$ (see figure 4). The phonon state density is of course highest in the most symmetrical points (Γ, K and M) corresponding to the centre and boundaries of the Brillouin zone of D_{6h}^4 phase, as should be expected. Just these phonons have to yield the most intense spectral lines. Starting from this assumption, an assignment of low-frequency

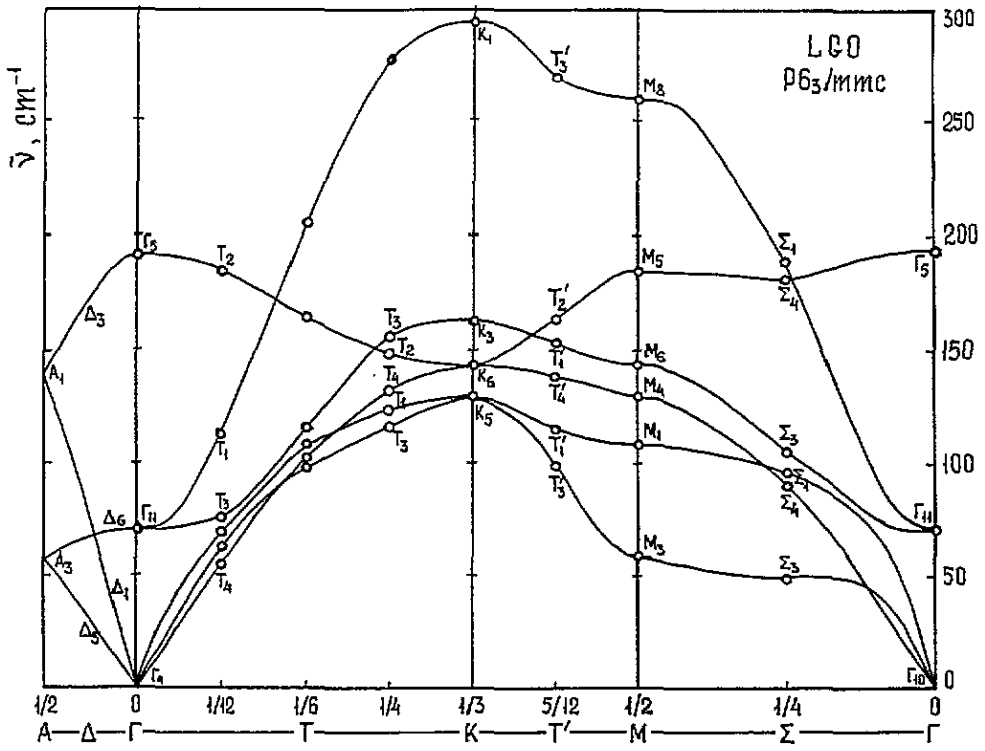

Figure 7. Possible arrangement of dispersion curves for the proptotype phase (aristotype) of LGO, as obtained by group theory with the use of the elastic constants of LGO at 300 K.

room-temperature spectra of LGO (up to 300 cm^{-1}) can be performed. In accord with correlations in figures 4 and 7, 18 totally symmetric A_g modes should be observed below 300 cm^{-1}; five of them are intense and originate from Γ_{11}, K_1, K_5, M_1 and M_5 modes of the prototypic phase. In correspondence with figure 5, we assign to them the lines with frequencies 68, 287 (or 260), 131, 111 and 186 cm^{-1}, respectively. As follows from figure 5 and table 4, the total number of A_g lines observed in our experiment equals practically that expected in this spectral range. Actually, after the transition owing to changes of mode symmetry and selection rules, arising structural deformations, etc, the picture we got by a 'direct mapping' of the branches of the prototypic phase onto the D_{2h}^{14} Brillouin zone spoils in comparison with the situation depicted in figure 9. At that it can also be expected that a redistribution of mode strengths and degeneracy lifting (increasing as the structure retracts from the transition point) will take place due to interactions between modes of identical symmetry.

In off-diagonal Raman spectra where modes with B_{ig} ($i = 1$–3) symmetry are active, seven or eight strong lines (we suppose their origin to be also in Γ, K and M modes) are observed; together with the number of weak lines observed, we again have the total number of lines close to that expected (18 lines each). Thus the room-temperature Raman spectra of LGO up to 300 cm^{-1} are very well assigned as originating from modes of close-packed oxygen layers of the prototypic phase.

Unfortunately, there is a much lower number of modes seen in IR spectra in comparison with the number of modes expected (18 for each orientation; see figure 6 and table 4). In the

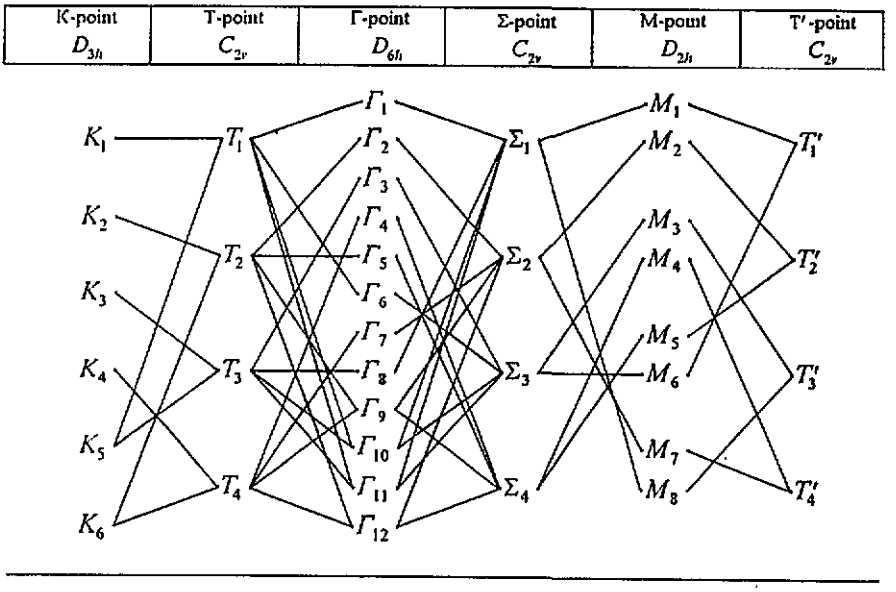

Figure 8. Compatibility relations between irreducible representations of D_{6h}^4 space group for the T and Σ directions.

light of the aforesaid, however, we can account for the fact that LGO remains practically IR-transparent up to 150 cm^{-1}: in accord with the picture of the dispersion and the correlations (see figure 7 and 4), Γ and M points of the phase D_{6h}^4 do not yield IR-active phonons in Γ point of D_{2h}^{14} (M_4, M_6, M_8 and K_i modes that yield IR-active phonons at the $D_{6h}^4 \rightarrow D_{2h}^{14}$ transition lie above 130 cm^{-1}).

The IR strength of modes originating from T_i and Σ_i modes of acoustic branches should be low due to the smallness of corresponding induced dipole moments. Table 4 presents a suggested relative genesis of Raman and IR lines observed in LGO. We however are not bold enough to state that it reflects the reality unambiguously.

One point (we think it very important) related to description of the ferroelectric phase transition should be dealt with here. It is the origin of the soft mode responsible for this phase transition. According to experimental data [3–7], the soft mode symmetry of the $D_{2h}^{14} \rightarrow C_{2v}^5$ transition at 283.5 K is B_{1u}. As follows from figure 7 and correlations in figure 4, out of the lowest-frequency modes, phonons of such symmetry can originate from phonons of acoustic branches T_4 ($q = \frac{1}{12}(b_1 + b_2)$), $T_3(q = \frac{1}{6}(b_1 + b_2))$, K_5, M_4 and Σ_3. Having selected the order parameter describing the $D_{6h}^4 \rightarrow D_{2h}^{14}$ phase transition, we showed that the Σ_3 mode of D_{6h}^4 phase is the necessary component of this order parameter. This mode splits into A_g and B_{1u} modes in D_{2h}^{14} and the shifts of oxygens in close-packed layers (O2–O5, O7, O8) correspond to this fact; the situation seems to disagree with neutron scattering data for $D_{2h}^{14} \rightarrow C_{2v}^5$ phase transition, which show the largest shifts for O1 and O6. We suppose that these large shifts occur as a consequence of 'sensitivity' of O1 and O6 to changes in oxygen packing within the layers. There, (even small) shifts corresponding to the soft mode may cause considerable rearrangements of built-in ions (Li2 and O1, O6) into the (a) sites. Large positional changes of Li2 and O1, O6 may be in principle considered as connected with the order–disorder transition. We will deal with this point in detail in connection with temperature behaviour of spectra at the ferroelectric phase transition.

Let us discuss briefly the high-frequency spectra. As shown above, isolated structural

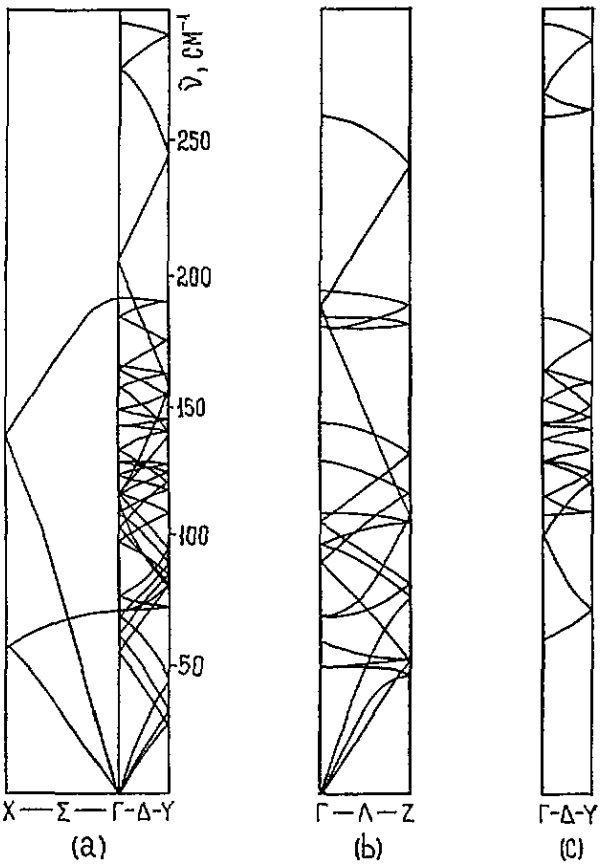

Figure 9. Schematic representation of the folding to the *Pbcn* Brillouin zone. Note that the perturbation induced by the formation of superlattice is small in this case.

fragments occurring in other substances can be extricated from the LGO structure. For example, the chemical formula of LGO can be written as $Li_2[Ge(Ge_2O_5)_3]$, which (if one adopts a substitution $O \rightarrow Ge_2O_5$) is an analogue of Li_2GeO_3, a crystal whose dynamics is well studied [21, 22]. These two substances contain infinite chains composed of GeO_3 ($Ge(Ge_2O_5)_3$) groups, with mutually close lengths of Ge–O bonds. ScO_6 octahedra in germanates with a thortveitite structure ($Sc_2Si_2O_7$) are analogous to GeO_6 and LiO_6 octahedra in LGO, which may serve as another example; the same applies to Ge_2O_7 bitetrahedra joined together into antiprisms. Here again the bond lengths are close to one another. Because of this similarity we suppose that high-frequency lines in LGO spectra may be assigned with the help of experimental and calculated data for these 'analogues'. We thus carried out a relative assignment of the high-frequency spectral lines by comparing LGO spectra with those of Li_2GeO_3 and $Sc_2Ge_2O_7$ [22, 23] (see table 5). This assignment undoubtedly is highly speculative and theoretical model calculation of spectra is necessary. Some conclusions, apparently correct, may nonetheless be arrived at. It is obvious that there is a strong mixing of some 'internal' (in principle bending) vibrations of complex anion with external lattice vibrations in LGO, at least below 550 cm^{-1}. The extent of this mixing depends substantially not only on the frequency but on the type of vibration as well. In the high-frequency region (800–1000 cm^{-1}) the mixing of internal vibrations with

lattice vibrations is insignificant. Shifts the atoms undergo at phase transitions may be accompanied not only with changes of orientations of a complex ion and its deformations, but with conformational changes as well; all this will strongly affect even frequencies of stretching vibrations. In the next paper of this series (devoted to ferroelectric transition in LGO) we will show that such phenomena really occur in LGO.

Table 5. Frequencies of lines in the Raman and IR spectra of LGO single crystals at room temperature and their assignment to the type of vibrations of molecular bond.

	A_g		B_{1g}	B_{2g}	B_{3g}	B_{1u}	B_{2u}	B_{3u}	
α_{aa}	α_{bb}	α_{cc}	α_{ab}	α_{ac}	α_{bc}	$E\|\|c$	$E\|\|b$	$E\|\|a$	Assignments
—	313	309	314	—	311	—	—	303	
—	—	322	324	327	—	—	—	—	δ(OGeO)
332	332	—	—	—	—	—	334	337	ν(LiO)
—	—	356	—	—	350	353	—	344	
366	368	368	366	367	—	—	364	—	ρ(GeOGe)
389	391	389	388	390	389	381	381	377	
420	422	421	—	418	422	—	410	—	
—	—	—	440	sh	446	458	458	436	
472	475	475	472	473	474	480	—	491	ν(GeOGe)
—	—	—	500	503	514	521	516	—	
540	542	542	—	545	545	—	—	—	
sh	—	549	549	—	556	558	555	—	
—	—	—	—	—	568	—	—	—	
583	—	—	—	—	—	579	—	—	
605	—	—	—	608	—	—	—	—	
—	793	794	—	791	788	784	—	—	
—	800	799	797	—	—	799	797	—	$\nu_{as}(GeO_3)$
—	—	—	—	—	831	—	—	—	
—	846	—	sh	sh	845	—	—	—	
—	855	853	858	856	860	855	854	—	ν_{as}(GeOGe)
—	—	—	911	903	893	907	890	—	
923	923	922	—	—	—	—	907	—	$\nu_s(GeO_3)$
sh	sh	—	938	949	—	935	—	—	

Isotopic studies of Li_2GeO_3 (^6Li, ^7Li) yielded the localization of Li lines: 250–500 cm^{-1}. Thus, the lowest-frequency band at about 490 cm^{-1} of stretching vibrations of anion ν_s–(Ge–O–Ge of the A_1 type) is 'hidden' among numerous bands of Li–O vibrations and, apparently, GeO_6 octahedra vibrations. At low temperatures this region really splits into many isolated lines.

Analysing the formation of room-temperature spectra of LGO from the standpoint of prototypic phase requires one to 'specify' (calculate) the following optical branches in the frequency region above 300 cm^{-1}: two $\Gamma_4 - \Sigma_4 - M_4$, two $\Gamma_{10} - \Sigma_1 + \Sigma_3 - M_8 + M_6$, $\Gamma_8 - \Sigma_1 - M_8$, $\Gamma_{12} - \Sigma_2 + \Sigma_4 - M_2 + M_4$, $\Gamma_5 - \Sigma_4 - M_5$ and $\Gamma_{11} - \Sigma_1 + \Sigma_3 - M_1 + M_3$ for the Γ–Σ–M direction, and the corresponding branches for the Γ–T–K direction (two $\Gamma_4 - T_4 - K_4$, two $\Gamma_{10} - T_1 + T_3 - K_5$, $\Gamma_8 - T_3 - K_3$, $\Gamma_{12} - T_2 + T_4 - K_6$, $\Gamma_5 - T_2 - K_2$ and $\Gamma_{11} - T_1 + T_3 - K_5$). One-half of these branches, however, belongs to voids. It is further required to map these branches onto the *Pbcn* Brillouin zone. At this stage of analysis, i.e. without results of numerical calculations of these dispersion branches, the solution for this problem is not yet possible.

5. Conclusions

In this work we have (i) constructed a prototypic phase of hexagonal symmetry for the weak ferroelectric LGO; (ii) described a hypothetical order–disorder phase transition with the order parameter transforming according to reducible representation $T_2 \oplus \Sigma_3$; and (iii) shown that the Σ_3 fraction of this order parameter may be taken as the precursor of the soft B_{1u} ferroelectric mode carrying a small charge.

Acknowledgments

The work was supported by the Grant No 93-02-15912 of the Russian Foundation for Fundamental Research. FK, FS and JP acknowledge the support of the Grant Agency of the Czech Republic (Project No 202/95/1393).

References

[1] Tagantsev A K, Sinii I G and Prokhorova S D 1987 *Izv. Akad. Nauk SSSR, Ser. Fiz.* **51b** 2089–92 (Engl. Transl. *Bull. Acad. Sci. USSR Phys. Ser.* **51** No 12 1)
[2] Haussuhl S, Wallrafen F, Recker K and Eckstein J 1980 *Z. Kristallogr.* **153** 329–37
[3] Wada M, Sawada A and Ishibashi Y 1981 *J. Phys. Soc. Japan* **50** 1811–12
[4] Orihara H, Wada M and Ishibashi Y 1983 *J. Phys. Soc. Japan* **52** 1478–84
[5] Volkov A A, Kozlov G V, Goncharov Yu G, Wada M, Sawada A and Ishibashi Y 1985 *J. Phys. Soc. Japan* **54** 818–21
[6] Sawada A, Wada M, Fujita K and Tiobana H 1985 *Japan. J. Appl. Phys. Suppl.* **24** 534–5
[7] Morioka Y, Wada M and Sawada A 1988 *J. Phys. Soc. Japan* **57** 3198–203
[8] Sinii I G, Fedoseev A I and Volnyanskii M D 1990 *Fiz. Tverd. Tela* **32** 353–63 (Engl. Transl. *Sov. Phys.–Solid State* **32** 202)
[9] Shitov G Yu, Timonin P N, Torgashev V I, Latush L T, Yuzyuk Yu I and Volnyanskii M D 1994 *Phase Transitions* **46** 143–61
[10] Strukov B A, Kozhevnikov M, Nizimov H A and Volnyanskii M D 1993 *Ferroelectrics* **143** 123–33
[11] Wada M and Ishibashi Y 1983 *J. Phys. Soc. Japan* **52** 193–9
[12] Bush A A and Venevtsev Yu N 1986 *Fiz. Tverd. Tela* **28** 1970–5 (Engl. Transl. *Sov. Phys.–Solid State* **28** 1101)
[13] Sawada A and Tomatsu M 1992 *Ferroelectrics* **137** 297–302
[14] Völlenkle H, Wittman A and Nowotny H 1970 *Monatsh. Chem.* **101** 45–56
[15] Gufan Yu I, Dimitriev V P, Roshal S B and Snezhkov V I 1990 *Landau Phases in Close-Packed Structures* (Rostov-on-Don: Rostov State University) (in Russian)
[16] Kovalev O V 1965 *Irreducible Representations of the Space Groups* (New York: Gordon and Breach)
[17] Koster G F 1957 Space groups and their representations *Solid State Physics* vol 5, ed F Seitz and D Turnbull (New York: Academic) p 173
[18] Lazarev A N, Mirgorodskii A P and Ignat'ev I S 1975 *Kolebatel'nye Spektry Slozhnykh Okislov. Silikaty i ikh Analogi* (Leningrad: Nauka) (in Russian)
[19] Torgashev V I, Latush L T and Yuzyuk Yu I 1992 *Ferroelectrics* **125** 129–34
[20] Iwata Y, Shibuya I, Wada M, Sawada A and Ishibashi Y 1987 *J. Phys. Soc. Japan* **56** 2420–7
[21] Orel B, Klanisek M, Moiseenko V, Volnyanskii M, Le Calve N, Pasquier B and Novak A 1985 *Phys. Status Solidi* b **128** 53–67
[22] Lazarev A N, Kolesova V A, Solnitseva L S and Mirgorodskii F P 1973 *Izv. Akad. Nauk. SSSR Neorg. Mater.* **9** 1969–75
[23] Lazarev A N and Mirgorodskii F P 1971 *Izv. Akad. Nauk SSSR Neorg. Mater.* **7** 1224–36
[24] Kadlec F, Petzelt J, Železný V and Volkov A A 1995 *Solid State Commun.* **94** 725–9